# Stability, Structure, and Binding Energies of Solvated Cluster Ions: Ammonia–Acetonitrile and Ammonia–Acetaldehyde Systems

W. B. Tzeng, S. Wei, and A. W. Castleman, Jr.*

*Department of Chemistry, The Pennsylvania State University, University Park, Pennsylvania 16802*
*(Received: December 27, 1990)*

Neutral ammonia–acetonitrile and ammonia–acetaldehyde mixed clusters, prepared in a pulsed nozzle supersonic expansion, are ionized by multiphoton ionization and investigated with a reflectron time-of-flight mass spectrometry technique. The observed mixed cluster ions $\{(NH_3)_n\cdot(M)_m\}H^+$, M = $CH_3CN$ and $CH_3CHO$, display a maximum intensity at $n + m = 5$, indicating that the cluster ions of $n + m = 5$ have a stable fully solvated shell structure. Studies of metastable unimolecular dissociation processes reveal that $\{(NH_3)_n\cdot(M)_m\}H^+$, $n = 1$, $m = 2$–4 lose one M molecule, whereas the mixed cluster ions of $n = 2$–11, $m = 1$–4 lose one $NH_3$ moiety in a sampled time window of a few tens of microseconds. The results support a proposed structure of the $\{(NH_3)_n\cdot(M)_m\}H^+$ cluster ions having a central species $NH_4^+$, to which the other ligands making up to the cluster are bound. This proposed structure of $\{(NH_3)_n\cdot(M)_m\}H^+$ can be interpreted through considerations of proton affinity, ion–dipole, and ion–induced dipole interaction. Bond energy measurements are reported for ammonia molecules bound to the ion $\{(NH_3)_nCH_3CN\}H^+$, for $n = 3$–10.

## Introduction

Upon ionization, clusters undergo internal ion–molecule reactions that lead to internal excitation and ultimately dissociation.[1-3] As a result, cluster ions of various sizes are created through rapid bond cleavage and fragmentation. Multiphoton ionization[3,4] provides a convenient way of ionizing neutral clusters, and study of the resulting dissociations and metastable dissociation processes can give insight into structures of the cluster ions.[3,5-10] Although various ion detection techniques are available for their study, a time-of-flight mass spectrometer (TOFMS) in conjunction with a reflectron allows one to detect the complete ensemble of cluster ions without size discrimination in less than a millisecond. In addition, metastability of evaporative cluster ions can be investigated.

Currently, there is considerable interest in the structure of protonated cluster ions and especially in the nature of the core ion. Stable structures of cluster ions have been proposed based on thermochemical considerations[11-13] and information on relative cluster ion intensity.[14-17] Studies of hydrogen-bonded mixed cluster ion systems containing water have raised an interesting question concerning whether the $H_3O^+$ is the central ion. It has been proposed that the stable cluster ions $(CH_3CN)_3(H_2O)H^+$ and $(CH_3OCH_3)_3(H_2O)H^+$ possess a $H_3O^+$ core ion but that the stable $(CH_3OH)_3(H_2O)H^+$ does not have a central hydronium ion.[18-23]

In the case of mixed cluster ions containing ammonia, we have recently found that $\{(NH_3)_n(CH_3COCH_3)_m\}H^+$, $n + m = 5$, form a solvation shell with a central species $NH_4^+$.[24,25] Neat clusters of ammonia,[11,16,26-38] acetonitrile,[17,18,39,40] and acetaldehyde[41,42]

(1) Klots, C. E.; Compton, R. N. *J. Chem. Phys.* **1978**, *69*, 1644.
(2) Garvey, J. F.; Bernstein, R. B. *J. Phys. Chem.* **1986**, *90*, 3577.
(3) Echt, O.; Dao, P. D.; Morgan, S.; Castleman, A. W., Jr. *J. Chem. Phys.* **1985**, *82*, 4076.
(4) Boesl, U.; Neusser, H. J.; Weinkauf, R.; Schlag, E. W. *J. Phys. Chem.* **1982**, *86*, 4857.
(5) Tai, T. L.; El-Sayed, M. A. *J. Phys. Chem.* **1990**, *90*, 4477.
(6) Morgan, S.; Castleman, A. W., Jr. *J. Am. Chem. Soc.* **1987**, *109*, 2867. Morgan, S.; Keesee, R. G.; Castleman, A. W., Jr. *J. Am. Chem. Soc.* **1989**, *111*, 3841.
(7) Breen, J. J.; Tzeng, W. B.; Kilgore, K.; Keesee, R. G.; Castleman, A. W., Jr. *J. Chem. Phys.* **1989**, *90*, 19.
(8) Tzeng, W. B.; Wei, S.; Castleman, A. W., Jr. *J. Am. Chem. Soc.* **1989**, *111*, 6035.
(9) Köhlewind, K.; Neusser, H. J.; Schlag, E. W. *Int. J. Mass Spectrom. Ion Phys.* **1983**, *51*, 255.
(10) Börnsen, K. O.; Lin, S. H.; Selzle, H. L.; Schlag, E. W. *J. Chem. Phys.* **1989**, *90*, 1299.
(11) Hogg, A. M.; Haynes, R. M.; Kebarle, P. *J. Am. Chem. Soc.* **1966**, *88*, 28.
(12) Grimsrud, E. P.; Kebarle, P. *J. Am. Chem. Soc.* **1973**, *95*, 7939.
(13) Lau, Y. K.; Saluja, P. P. S.; Kebarle, P. *J. Am. Chem. Soc.* **1980**, *102*, 7429.
(14) Searcy, J. Q.; Fenn, J. B. *J. Chem. Phys.* **1974**, *61*, 5282.
(15) Stace, A. J.; Shukla, A. K. *J. Am. Chem. Soc.* **1982**, *104*, 5314.
(16) Echt, O.; Morgan, S.; Dao, P. D.; Stanley, R. J.; Castleman, A. W., Jr. *Ber. Bunsen-Ges. Phys. Chem.* **1984**, *88*, 217.
(17) Mestdagh, J. M.; Binet, A.; Sublemontier, O. *J. Phys. Chem.* **1989**, *93*, 8300.
(18) Meot-Mer, M. *J. Am. Chem. Soc.* **1980**, *100*, 4694.
(19) Deakyne, C. A.; Meot-Ner, M.; Campbell, C. L.; Hughes, M. G.; Murphy, S. P. *J. Chem. Phys.* **1986**, *84*, 4958.
(20) Stace, A. J.; Moore, C. *J. Phys. Chem.* **1982**, *86*, 2681.
(21) Böhringer, H.; Arnold, F. *Nature* **1981**, *290*, 321.
(22) Nishi, N.; Yamamoto, K.; Shinohara, H.; Nagashima, U.; Okuyama, T. *Chem. Phys. Lett.* **1985**, *122*, 599.
(23) Iraqi, M.; Lifshitz, C. *Int. J. Mass Spectrom. Ion Proc.* **1986**, *71*, 245. Graul, S. T.; Squires, R. R. *Int. J. Mass Spectrom. Ion Proc.* **1989**, *94*, 41.
(24) Tzeng, W. B.; Wei, S.; Neyer, D. W.; Keesee, R. G.; Castleman, A. W., Jr. *J. Am. Chem. Soc.* **1990**, *112*, 4097.
(25) Tzeng, W. B.; Wei, S.; Castleman, A. W., Jr. *Chem. Phys. Lett.* **1990**, *166*, 343.
(26) Long, J. W.; Franklin, J. L. *Int. J. Mass Spectrom. Ion. Phys.* **1973**, *12*, 403.
(27) Lindinger, W.; Albritton, D. L.; Fehsenfeld, F. W.; Schmeltekopf, A. L.; Ferguson, E. E. *J. Chem. Phys.* **1975**, *62*, 3549.
(28) Tang, I. N.; Castleman, A. W., Jr. *J. Chem. Phys.* **1975**, *62*, 4579. Futrell, J. H.; Stephan, K.; Märk, T. D. *J. Chem. Phys.* **1982**, *76*, 5893.
(29) Ceyer, S. T.; Tiedemann, P. W.; Mahan, B. H.; Lee, Y. T. *J. Chem. Phys.* **1979**, *70*, 14.
(30) Hirao, K.; Fujikawa, T.; Konishi, H.; Yamabe, S. *Chem. Phys. Lett.* **1984**, *104*, 184.
(31) Shinohara, H.; Nishi, N.; Washida, N. *Chem. Phys. Lett.* **1984**, *106*, 302.
(32) Fraser, G. T.; Nelson, D., Jr.; Charo, A.; Klemperer, W. *J. Chem. Phys.* **1985**, *82*, 2535.
(33) Kreisle, D.; Leiter, K.; Echt, O.; Märk, T. D. *Z. Phys. D* **1986**, *3*, 319.
(34) Price, J. M.; Crofton, M. W.; Lee, Y. T. *J. Chem. Phys.* **1989**, *91*, 2749.
(35) Wei, S.; Tzeng, W. B.; Castleman, A. W., Jr. *J. Chem. Phys.* **1990**, *92*, 332.
(36) Wei, S.; Tzeng, W. B.; Castleman, A. W., Jr. *J. Chem. Phys.* **1990**, *93*, 2507.
(37) Peifer, W. R.; Coolbaugh, M. T.; Garvey, J. F. *J. Chem. Phys.* **1989**, *91*, 6684.
(38) Lifshitz, C.; Louage, F. *J. Phys. Chem.* **1989**, *93*, 5633. Buck, U.; Lauenstein, Ch. *J. Chem. Phys.* **1990**, *92*, 4250.

0022-3654/91/2095-5757$02.50/0 

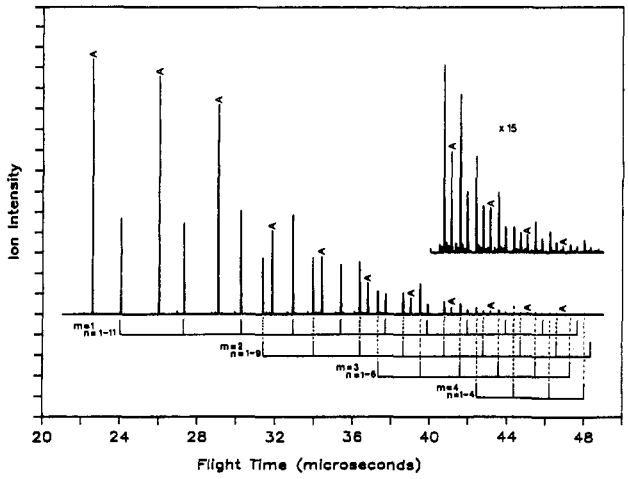


**Figure 1.** TOF spectrum of $\{(NH_3)_n\cdot(CH_3CN)_m\}H^+$; $U_0$ = 2460 V; $U_t$ = 2900 V; A ≡ $(NH_3)_nH^+$, $n$ = 3–13.

have been studied extensively, but the mixed ammonia–acetonitrile and ammonia–acetaldehyde clusters have received little attention. This paper represents part of our continuing study of stability, structure, and dissociation dynamics of mixed cluster ions containing ammonia and other substances with attention to systems with widely varying proton affinities.

## Experimental Section

The apparatus used in these studies has been described in previous publications.[8,24] In brief, the mixed neutral clusters are made by expanding a gas vapor containing ammonia and acetonitrile (or acetaldehyde) through a pulsed nozzle (diameter = 150 μm) at a pressure of 2–4 atm. The gas mixture is prepared in a container so that the mixing ratios can be easily varied according to their partial pressures. The mixed neutral clusters are ionized by 355-nm light from a frequency-tripled Nd:YAG laser. The product ions formed by multiphoton ionization are accelerated by a double electrostatic field (TOF lens) to about 2.6 keV and directed through a 130-cm-long field-free region toward a reflectron. Ions are then reflected at a small angle of about 3° and thereafter travel 80 cm through another field-free region toward a chevron microchannel plate ion detector. The signal received by the detector is fed into a 100-MHz transient recorder coupled to an IBM PC/AT computer. The experiments operate at 10 Hz, and TOF spectra typically are accumulated for 1000 laser shots.

In the present experiments, the mixed cluster size distribution was independent of the nozzle stagnation pressure in the range 1600–3200 Torr and also independent of the laser power for values of 15–60 mJ/pulse. Therefore, the nozzle stagnation pressure was typically set at 2400 Torr, and the laser power was held at 25 mJ/pulse for these experiments. The initial parent ion energy ($U_0$), established by potentials applied to the TOF lens elements, was measured by using the reflectron as an energy analyzer. A "hard reflection" TOF spectrum (e.g., Figure 1) can be obtained when the voltage applied to the second plate of the reflectron unit ($U_t$) is set higher than the initial parent ion energy, $U_0$. The pressure in the field-free and ion detector regions is maintained below $4 \times 10^{-7}$ Torr during normal operation. Experiments have been conducted to ensure that collision-induced dissociation of the cluster ions is negligible.[8,35] When a metastable parent ion decomposes to a daughter ion and a neutral species, the daughter ion has an energy of $U_d = (M_d/M_p)U_0$, where $M_d$ and $M_p$ are masses of daughter and parent ions, respectively. A TOF spectrum containing daughter ion peaks, while excluding parent ions, is obtained when $U_t$ is set slightly lower than the initial parent ion energy $U_0$.

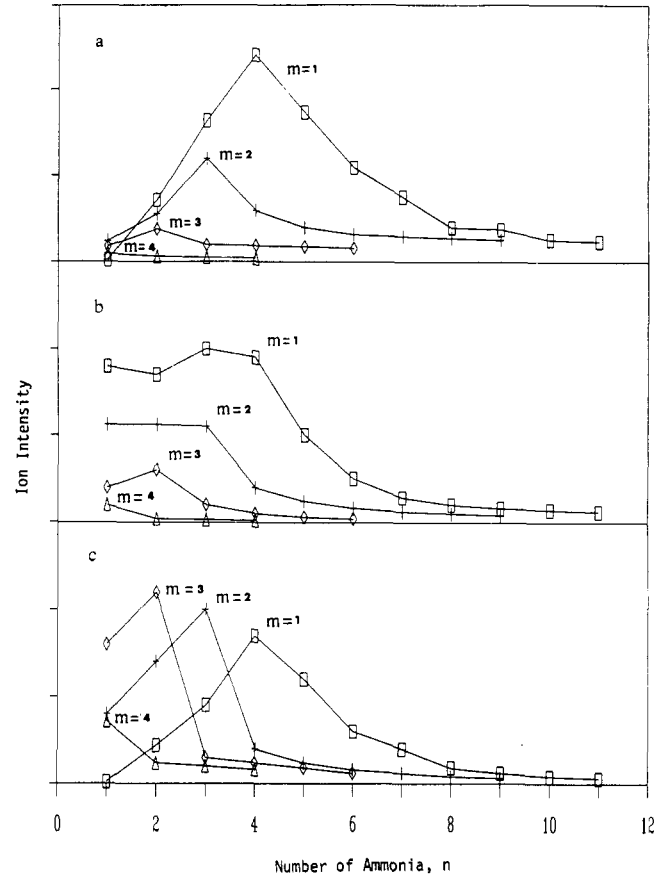


**Figure 2.** Plot of relative ion intensity of $\{(NH_3)_n\cdot(CH_3CN)_m\}H^+$ as $n$ for $m$ = 1–4; $R$ = acetonitrile/ammonia. (a) $R$ = 1/2400; (b) $R$ = 10/2400; (c) $R$ = 100/2400.

The ammonia (anhydrous, minimum purity of 99.99%) used in these experiments was obtained from Linde Specialty Gases. The acetonitrile liquid sample (purity of 99.9%) was purchased from EM Industries, Inc., whereas the acetaldehyde was a certified ACS spectranalyzed grade obtained from Fisher Scientific. All chemicals were used without further purification.

## Results

**I. Ammonia–Acetonitrile Clusters. (A) Hard Reflection Time-of-Flight Spectrum.** Figure 1 shows a portion of a typical hard reflection TOF spectrum of ammonia–acetonitrile cluster ions taken under conditions where the gas vapor behind the pulsed nozzle had a mixing ratio of acetonitrile/ammonia $R$ = 1/240. The observed cluster ions are $(NH_3)_nH^+$ (designated as A) and $\{(NH_3)_n\cdot(CH_3CN)_m\}H^+$ (labeled with $n$, $m$). The ion intensity distribution of $(NH_3)_nH^+$ is similar to that observed in the multiphoton ionization of neat ammonia clutsers.[16,35,36] An abrupt decrease in the intensity of $(NH_3)_nH^+$ between $n$ = 5 and $n$ = 6 indicates that the cluster ion $(NH_3)_4\cdot NH_4^+$ is a relatively stable species. The structure of $(NH_3)_4\cdot NH_4^+$ can be pictured as a central ammonium ion $NH_4^+$ bound to four $NH_3$ molecules.[16,35]

The ratio of gas components in the gas vapor is crucial for the formation of mixed neutral clusters of various sizes using this coexpansion method.[15,17,24] It is important to investigate how the gas component ratio affects the cluster ion intensity distribution. Figure 2 is a plot of relative intensity of cluter ions $\{(NH_3)_n\cdot(CH_3CN)_m\}H^+$ as a function of $n$ for each $m$ = 1–4 for acetonitrile/ammonia ratio ($R$) ranged from 1/2400 to 100/2400. At $R$ = 1/2400, a local maximum at $m + n$ = 5 is seen as shown in Figure 2a. Intensities of larger cluster ions (higher m value) are quite small due to the fact that there are fewer neutral ammonia–acetonitrile clusters available for forming mixed cluster ions upon photoionization. When $R$ is increased to 10/2400, a sharp drop in the ion intensity of $\{(NH_3)_n\cdot(CH_3CN)_m\}H^+$ between

(39) Hirao, K.; Yamabe, S.; Sano, M. *J. Phys. Chem.* **1982**, *86*, 2626. Al-Mubarak, A. S.; Mistro, G. D.; Lethbridge, P. G.; Abduh-Sattar, N. Y.; Stace, A. J. *Faraday Discuss. Chem. Soc.* **1988**, *86*, 209.
(40) Illies, A. J. *Org. Mass Spectrom.* **1989**, *24*, 186.
(41) Krassig, R.; Reinke, D.; Baumgartel, H. *Ber. Bunsen-Ges. Phys. Chem.* **1974**, *78*, 425.
(42) Tzeng, W. B.; Wei, S.; Castleman, A. W., Jr. *Chem. Phys. Lett.* **1990**, *168*, 30.

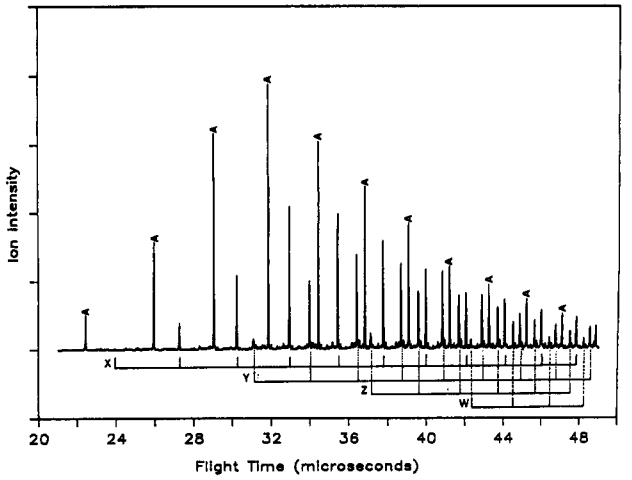


**Figure 3.** Daughter ion TOF spectrum of $\{(NH_3)_n\cdot(CH_3CN)_m\}H^+$; $U_t$ = 2430 V. X, Y, Z, and W stand for daughter ion peaks with their corresponding parent ions $\{(NH_3)_n\cdot(CH_3CN)_m\}H^+$, $m$ = 1–4, respectively. The metastable unimolecular decomposition processes expressed as (2) and (3) as discussed in the text.

$n + m = 5$ and $n + m = 6$ is evident in Figure 2b. As shown in Figure 2c, the relative intensities of $\{(NH_3)_n\cdot(CH_3CN)_m\}H^+$ of larger $m$ become distinct as $R$ is increased to 100/2400. This result can be accounted for by the fact that more neutral ammonia–acetonitrile clusters are formed through the supersonic expansion. Another observation in Figure 2c is a local maximum at $m + n = 5$ in the intensity of the ions $\{(NH_3)_n\cdot(CH_3CN)_m\}H^+$, $m$ = 1–4. The above observations of distinct features in the ion intensity distributions of $\{(NH_3)_n\cdot(CH_3CN)_m\}H^+$ in all gas vapors of different acetonitrile/ammonia mixing ratios indicate that the cluster ions $\{(NH_3)_n\cdot(CH_3CN)_m\}H^+$, $n + m = 5$, have a particularly stable configuration not dependent upon the distribution of the neutral clusters produced.

**(B) Daughter Ion Time-of-Flight Spectrum.** Figure 3 displays a reflectron TOF spectrum showing daughter ion peaks that result from unimolecular decompositions in the TOF field-free region. The daughter ion peaks labeled as A arise from the following unimolecular decomposition process:

$$(NH_3)_nH^+ \rightarrow (NH_3)_{n-1}H^+ + NH_3, \quad n = 3\text{–}13 \qquad (1)$$

When undergoing metastable unimolecular decomposition, the metastable cluster ions $\{(NH_3)_n\cdot(CH_3CN)_m\}H^+$ release the relatively loosely bound molecule. The daughter ion peaks labelled as X, Y, Z, and W in Figure 3 result from the parent ions $\{(NH_3)_n\cdot(CH_3CN)_m\}H^+$, $m$ = 1–4, respectively. Those corresponding to the parent ions $\{NH_3\cdot(CH_3CN)_m\}H^+$, $m$ = 2–4, (first peak from left for each X, Y, Z, and W series in Figure 3) are shifted toward earlier times by about 0.2–0.3 μs with respect to their parent ion arrival times in Figure 1. This is due to the fact that the daughter ions have an energy $U_d = (M_d/M_p)U_0$ do not penetrate into the reflectron unit as deeply as do the parent ions. Thus, they spend less time in the reflectron (turn around earlier) compared to their parent ions which have an energy of $U_0$ and reach the detector earlier.

The daughter ion peaks corresponding to the parent ions $\{(NH_3)_n\cdot(CH_3CN)_m\}H^+$, $n$ = 2–11, $m$ = 1–4, (all but the first peaks from left in the X, Y, Z, and W series in Figure 3) are shifted toward earlier times by about 0.01–0.15 μs as compared to their parent ion arrival times in Figure 1. The smaller shifts in the ion arrival times as compared to the previous case (loss of $CH_3CN$, mass 41) is due to the smaller mass of the lost moiety $NH_3$ (mass 17). Therefore, the assignment of the daughter ion peaks can be done by comparing the difference in the daughter and parent ion arrival times.

The unimolecular decompositions of metastable cluster ions $\{(NH_3)_n\cdot(CH_3CN)_m\}H^+$ are confirmed by the daughter ion cutoff potential experiments in which the $U_t$ voltage is varied and the threshold for the disappearance of the daughter ion peaks is determined.[8,35] The initial parent ion energy $U_0$ has been measured

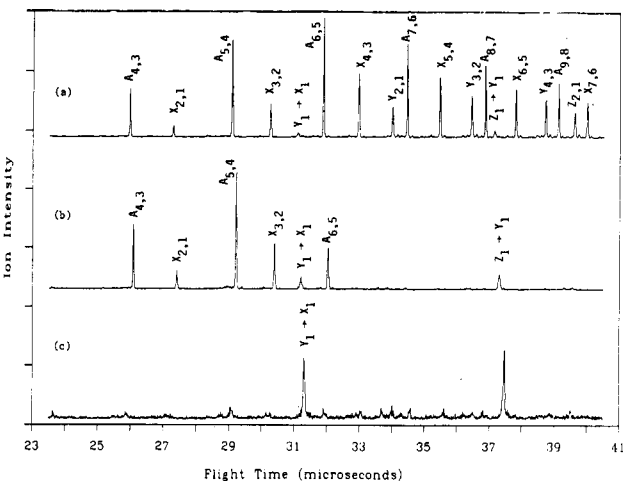


**Figure 4.** Daughter ion cutoff potential study. (a) $U_t$ = 2430; (b) $U_t$ = 2080 V; (c) $U_t$ = 1830 V.

**TABLE I: Daughter Ion Cutoff Potentials ($U_c$) of Metastable Decomposition Processes (1)–(3) in the Text and Observed Ion Peaks in Figure 4**

| parent ion | $U_c$, V | decomposition process | obsd moiety lost |
|---|---|---|---|
| $(NH_3)_4H^+$ | 1486 | 1 | $NH_3$ |
| $(NH_3)_5H^+$ | 1966 | 1 | $NH_3$ |
| $(NH_3)_6H^+$ | 2046 | 1 | $NH_3$ |
| $(NH_3)_7H^+$ | 2103 | 1 | $NH_3$ |
| $(NH_3)_8H^+$ | 2146 | 1 | $NH_3$ |
| $(NH_3)_9H^+$ | 2180 | 1 | $NH_3$ |
| $\{(NH_3)_2\cdot CH_3CN\}H^+$ | 1902 | 3 | $NH_3$ |
| $\{(NH_3)_3\cdot CH_3CN\}H^+$ | 2002 | 3 | $NH_3$ |
| $\{(NH_3)_4\cdot CH_3CN\}H^+$ | 2071 | 3 | $NH_3$ |
| $\{(NH_3)_5\cdot CH_3CN\}^+$ | 2122 | 3 | $NH_3$ |
| $\{(NH_3)_6\cdot CH_3CN\}H^+$ | 2161 | 3 | $NH_3$ |
| $\{(NH_3)_7\cdot CH_3CN\}H^+$ | 2191 | 3 | $NH_3$ |
| $\{NH_3\cdot(CH_3CN)_2\}^+$ | 1446 | 2 | $CH_3CN$ |
| $\{(NH_3)_2\cdot(CH_3CN)_2\}H^+$ | 2094 | 3 | $NH_3$ |
| $\{(NH_3)_3\cdot(CH_3CN)_2\}H^+$ | 2239 | 3 | $NH_3$ |
| $\{(NH_3)_4\cdot(CH_3CN)_2\}H^+$ | 2175 | 3 | $NH_3$ |
| $\{NH_3\cdot(CH_3CN)_3\}H^+$ | 1446 | 2 | $CH_3CN$ |
| $\{(NH_3)_2\cdot(CH_3CN)_3\}H^+$ | 2094 | 3 | $NH_3$ |

to be 2460 ± 10 V. Figure 4a is a replot of Figure 3, which is a TOF spectrum taken at $U_t$ = 2430 V. When the $U_t$ is lowered to 2080 V, only the peaks corresponding to yielding daughter ions with energy $(M_d/M_p)(2450) < 2080$ V can be seen, as shown in Figure 4b. When the $U_t$ is further lowered to 1830 V, only two peaks corresponding to decomposition process (2) for $m$ = 2 and 3 are observed. Table I lists the daughter ion cutoff potentials of observed metastable decomposition processes for further confirmation on the peak assignments in Figure 4. On the basis of our experimental results, the unimolecular decomposition processes of the metastable $\{(NH_3)_n\cdot(CH_3CN)_m\}H^+$ can be classified into two categories:

(a) $n$ = 1 and $m$ = 2–4:

$$\{(NH_3)_n\cdot(CH_3CN)_m\}H^+ \rightarrow \{(NH_3)_n\cdot(CH_3CN)_{m-1}\}^+ + CH_3CN \qquad (2)$$

(b) $n$ = 2–11, $m$ = 1–4:

$$\{(NH_3)_n\cdot(CH_3CN)_m\}H^+ \rightarrow \{(NH_3)_{n-1}\cdot(CH_3CN)_m\}H^+ + NH_3 \qquad (3)$$

Any given parent cluster ion $\{(NH_3)_n\cdot(CH_3CN)_m\}H^+$ shows evidence of dissociation only via one channel, either reaction 2 or 3, but not both in our observable time window.

**(C) Measurement of Average Kinetic Energy Release.** Measurement of the average kinetic energy release of metastable ions is based on a peak-shape analysis of the TOF spectra. The importance of using a reflectron time-of-flight mass spectrometer in the studies of metastable unimolecular dissociation dynamics lies in being able to measure both the dissociation rate[36] and the kinetic energy release.[35] This method was originally proposed by

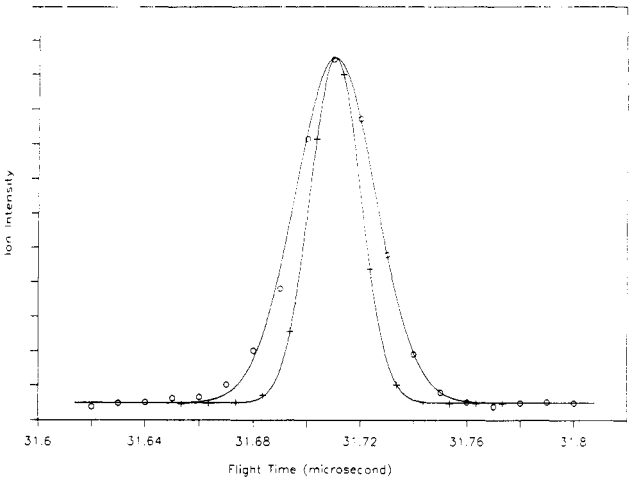


**Figure 5.** Experimental data points of the parent ion $\{(NH_3)_4CH_3CN\}H^+$ (designated as +) and the daughter ion $\{(NH_3)_3CH_3CN\}H^+$ (designated as O) fitted by Gaussian functions (solid line).

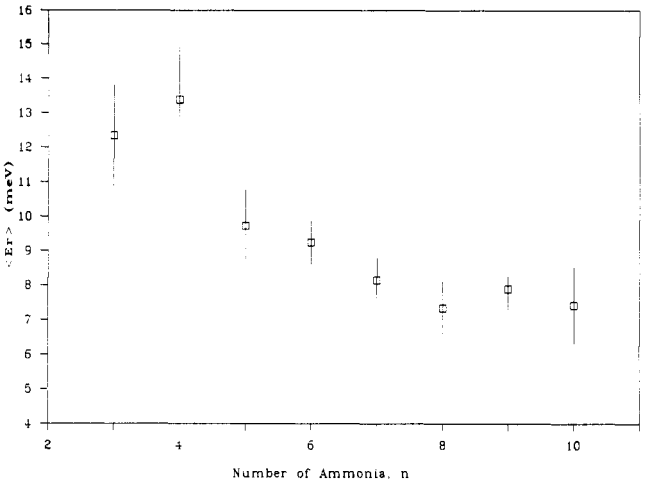


**Figure 6.** Plot of the measured average kinetic energy release during the metastable unimolecular decompositions of $\{(NH_3)_nCH_3CN\}H^+$, $n$ = 3–10, as a function of $n$.

Berry[50] and later developed by Franklin et al.[51] for use in a TOF mass spectrometer. During the decomposition of the metastable parent ion in the field-free drift region, the internal energy of the parent ion is converted to the translational energy of the daughter ion. As a result, the translational energy distribution of the daughter ion is expected to be broader than that of the parent ion due to the kinetic energy release in the decomposition process.

Baldwin et al.[52] pointed out that the broadening width $W_t$, resulting from the kinetic energy release can be obtained from the relationship $W_t^2 = W_d^2 - W_p^2$, where $W_d$ is the width of the daughter ion at 22% of the peak height, and $W_p$ is the width of the parent ion peak in the mass-selected ion kinetic energy spectra. The formula $W_t^2 = W_d^2 - W_p^2$ is exact only if both parent and daughter ion peak shapes are Gaussian.

With a measured parent ion birth potential $U_0$, an estimated daughter ion travelling distance in the field-free drift region, $L$ (distance from the position where the daughter ion is born to the ion detector), and a broadening width $W_t$ observed in the TOF spectra, the average kinetic energy release is given by[35]

$$\langle E_r \rangle = \frac{1}{\langle L^2 \rangle}(U_0 W_t)^2 \left( \frac{M_d}{2M_p M} \right) \qquad (4)$$

where $M_p$, $M_d$, and $M$ are the masses of parent ion, daughter ion, and neutral fragment, respectively.

In the present work, all parent and cluster ion peaks observed display a Gaussian shape in the TOF spectra, and this is the crucial requirement for the KER measurements. As an example, the experimental data points of the parent ion peak of $(NH_3)_3CH_3CNH^+$ (10 ns apart from each other, indicated as +) and the daughter ion $(NH_3)_3CH_3CNH^+$ (indicated as O) are fitted to the pure Gaussian curves (indicated as solid lines) as shown in Figure 5. Clearly, the daughter ion peak is broader than the parent ion peak due to kinetic energy release involved in the decomposition process. The complete KER results for the mixed cluster ions $(NH_3)_nCH_3CNH^+$ are plotted in Figure 6, along with the experimental error bars from 10 independent measurements.

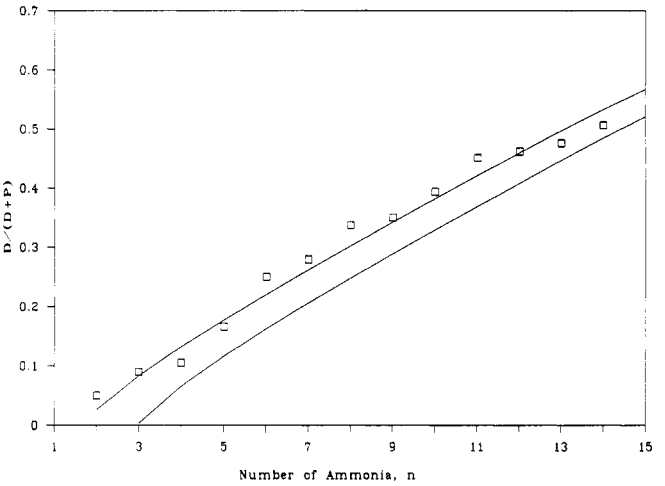


**Figure 7.** Plot of decay fraction of $\{(NH_3)_nCH_3CN\}H^+$, $n$ = 2–14, as a function of $n$. □ ≡ experimental values with an error of less than 5% for each value, this work; solid line ≡ theoretical value deduced from eq 5. The upper line is obtained when $C_n = [6(n-1) + 8]$; the lower line is obtained when $C_n = 6(n-1)$.

**(D) Determination of Binding Energies of $(NH_3)_nCH_3CNH^+$.** Klots[53] and Engelking[54] have independently developed evaporative ensemble and modified QET/RRK statistical models to account for the dynamics of unimolecularly dissociating cluster ions. The Klots' evaporative ensemble[53] assumes that each cluster ion has suffered at least one evaporation before entering the field-free region of the time-of-flight mass spectrometer. For each cluster ion, the flight time for the parent ion entering the field-free region is $t_0$, whereas $t$ is the flight time for the parent ion to reach the reflectron. The evaporative ensemble predicts that the normalized population of the daughter ions at $t$ is given[53,36] by

$$D = (C_n/\gamma'^2) \ln \{t/[t_0 + (t - t_0) \exp(-\gamma'^2/C_n)]\} \qquad (5)$$

where $C_n$ is the heat capacity of the cluster ion of size $n$ (in the units of Boltzmann constant), $\gamma'^2 = \gamma^2/[1 - (\gamma/2C_n)^2]$, and $\gamma$ is the Gspann parameter. In the above equation, the value of $t_0$ can be calculated by using a formula given by Wiley and McLaren,[55] and $t$ can be obtained from the TOF spectrum. Since the Gspann parameter is found to be ~25, the only unknown parameter that has to be determined here is the heat capacity $C_n$ which is obtained

(43) Cooks, R. G.; Beynon, J. H.; Caprioli, R. M.; Lester, G. R. *Metastable Ions*; Elsevier, Amsterdam, 1973.
(44) Meot-Ner, M. *J. Am. Chem. Soc.* **1984**, *106*, 1257.
(45) Lias, S. G.; Liebman, J. F.; Levin, R. D. *J. Phys. Chem. Ref. Data* **1984**, *13*, 695.
(46) Lias, S. G.; Bartmess, J. E.; Liebman, J. F.; Holmes, J. L.; Levin, R. D.; Wallard, W. G. *J. Phys. Chem. Ref. Data* **1988**, *17*, Suppl. No. 1.
(47) Keesee, R. G.; Castleman, A. W., Jr. *J. Phys. Chem. Ref. Data* **1986**, *15*, 1011.
(48) McMillen, D. F.; Golden, D. M. *Annu. Rev. Phys. Chem.* **1982**, *33*, 493.
(49) Applequist, J.; Carl, J. R.; Fung, K. K. *J. Am. Chem. Soc.* **1972**, *94*, 2952.
(50) Berry, C. E. *Phys. Rev.* **1950**, *78*, 597.
(51) Franklin, J. L.; Hierl, P. M.; Whan, A. A. *J. Chem. Phys.* **1967**, *47*, 3148.
(52) Baldwin, M. A.; Derrick, P. J.; Morgan, R. P. *Org. Mass Spectrom.* **1976**, *11*, 440.
(53) Klots, C. E. *J. Chem. Phys.* **1985**, *83*, 5853; *Z. Phys. D.* **1987**, *5*; *J. Phys. Chem.* **1988**, *92*, 5864.
(54) Engelking, P. C. *J. Chem. Phys.* **1986**, *85*, 3103; **1987**, *87*, 936.
(55) Wiley, W. C.; McLaren, I. H. *Rev. Sci. Instrum.* **1955**, *11*, 1150.

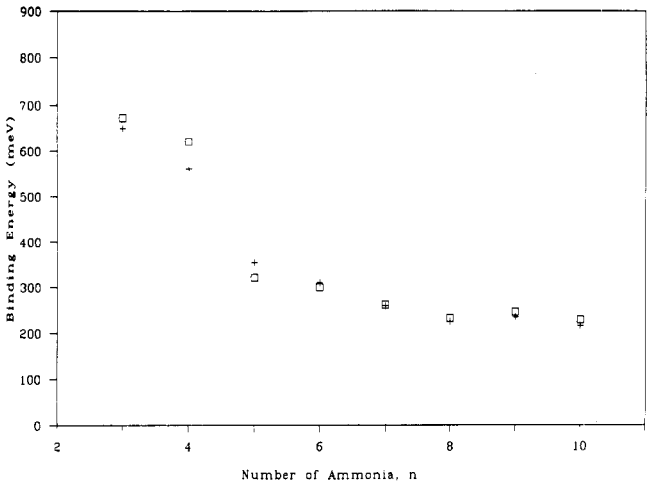


**Figure 8.** Plot of the calculated binding energies of ammonia to the cluster ions $\{(NH_3)_nCH_3CN\}H^+$, $n$ = 3–10, as a function of $n$. + ≡ deduced values using Klots' evaporative ensemble model; □ ≡ deduced values using Engelking's modified QET/RRK model.

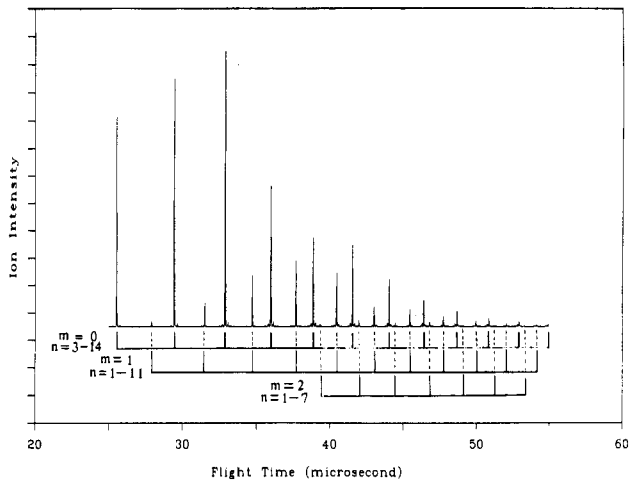


**Figure 9.** TOF spectrum of $\{(NH_3)_n\cdot(CH_3CHO)_m\}H^+$, $U_0$ = 1905 V; $U_t$ = 2600 V; A ≡ $(NH_3)_nH^+$, $n$ = 3–13.

from the measured decay fraction.

The decay fraction of the mixed cluster ions $(NH_3)_nCH_3CNH^+$ is measured from the integrated intensities of the parent and the daughter ion peaks in the TOF spectrum. Special care has been taken to improve the precision to the measurement concerning instrumental artifacts and the ion trajectories of the parent and daughter ions.[36] The results are shown in Figure 7 for the cluster ion $(NH_3)_nCH_3CNH^+$, $n$ = 2–14. To apply Klots' model, a function of $C_n \sim n$ has to be assumed, which is, of course, consistent with an increasing number of active modes with cluster size. Considering that the heat capacity is found to be $C_n = 6(n-1)$ for ammonia cluster ions $(NH_3)_nH^+$ (due to the cluster modes), the heat capacity is assumed as $C_n = \{6(n-1) + B\}$ for the cluster ions $(NH_3)_nCH_3CNH^+$ since one $CH_3CN$ molecule is added on to $(NH_3)_nH^+$. The best fit (the upper line in Figure 7) to the measured decay fraction is found when $B$ = 8, which indicates that two internal low-frequency modes (plus six cluster modes) of the $CH_3CN$ molecule are involved in the metastable decomposition process. As a comparison, the calculated values when $B$ = 0 are also shown (the lower line in Figure 7).

With the determined heat capacity and the measured KER, the binding energy can be calculated[53,36] by using the following equation:

$$\Delta E_n = \gamma\langle E_r\rangle/[1 - (\gamma/2C_n)] \quad (6)$$

The deduced binding energy is shown in Figure 8 (indicated as +). An abrupt decrease from $n$ = 4 to 5 is evident.

An altenative approach is to employ the modified QET/RRK theory proposed by Engelking. From metastable lifetime and average kinetic energy release, the binding energy of a molecule within a metastable cluster ion can be determined[54,35] as follows:

$$\Delta E_n = A(s-1)[C^{1/(s-1)}\langle E_r\rangle^{(s-2)/(s-1)} - \langle E_r\rangle] \quad (7)$$

where $s$ = number of the active modes, $A$ is the model scaling parameter (0.5 given by Engelking[54]), and $C = 16\pi\nu^3\mu gS/\Gamma_n$. To calculate the constant $C$, one needs to obtain information on $\nu$ (vibrational frequency of cluster mode), $\mu$ (reduced mass), $g$ (remaining channel degeneracy of the ejected neutral fragment), $S$ (geometrical cross section for forming cluster ion), and $\Gamma_n$ (unimolecular dissociation rate). Fortunately, the constant $C$ is taken to a large root $(1/(s-1))$. Hence, the choices of those parameters are not sensitive to the computed binding energies. For simplicity, the channel degeneracy $g$ and the vibrational frequencies are set to $n-1$ and 100 $cm^{-1}$, the geometrical cross section $S$ is chosen to be 100 $Å^2$, and the lifetimes $(1/\Gamma_n)$ of the metastable cluster ions are estimated from the observed ion arrival times.

The two parameters that have to be determined are the active modes $s$ and the scaling parameter $A$, which are sensitive to the results. The cluster modes of the cluster ion $(NH_3)_nCH_3CNH^+$ including rotations and translations of each monomer are treated as active, providing $6(n-1) + 6$ degrees of freedom. As seen from the studies of the decay fraction measurement discussed above, two internal modes of $CH_3CN$ are also involved in the decomposition process. Therefore, $s$ is taken to be $6(n-1) + 8$. From the studies of $(NH_3)_nH^+$, it is found the calculated binding energies are best fitted to the thermochemical values[35] when $A$ = 1. Considering the similarity of the two metastable process, $A$ is chosen as 1 for the parent case as well.

Applying the eq 7 and the measured KER, the binding energies are calculated; the results are presented in Figure 8 (indicated as □). Clearly, both models are in very good agreement.

**II. Ammonia–Acetaldehyde Clusters. (A) Hard Reflection Time-of-Flight Spectrum.** Figure 9 shows a portion of a typical hard reflection TOF spectrum of photoionized ammonia–acetaldehyde clusters taken at $U_t$ = 2600 V (higher than $U_0$). The stagnation pressure of the gas vapor behind the pulsed nozzle is 2400 Torr with a mixing ratio of acetaldehyde/ammonia = 4. The observed cluster ions are $(NH_3)_nH^+$ $\{(NH_3)_n\cdot(CH_3CHO)_m\}H^+$ (labeled with $n$, $m$). The influence of the gas components' relative composition on the mixed cluster ion intensity is also investigated. Figure 10 is a plot of the relative ion intensity of $\{(NH_3)_n\cdot(CH_3CHO)_m\}H^+$ as a function of the number $n$ of ammonia molecules for each $m$ = 1–2. A maximum intensity of the ions $\{(NH_3)_n\cdot(CH_3CHO)_m\}H^+$ at $n + m$ = 5 is found to be independent of the acetaldehyde/ammonia ($R$) mixing ratio from $R$ = 1/4 to 4. This indicates that the cluster ions $\{(NH_3)_n\cdot(CH_3CHO)_m\}H^+$, $n + m$ = 5, are relatively stable in a fashion similar to the acetonitrile–ammonia system.

**(B) Daughter Ion Time-of-Flight Spectrum.** Figure 11 displays a reflectron TOF spectrum showing daughter ion peaks for ammonia–acetaldehyde cluster system. The daughter ion peaks labeled as A result from the unimolecular decompositions of $(NH_3)_nH^+$ as expressed in process (1). The daughter ion peaks labelled as X, Y, Z, and W result from the parent ions $\{(NH_3)_n\cdot(CH_3CHO)_m\}H^+$, $m$ = 1–4, respectively. The observed unimolecular decomposition processes of the metastable $\{(NH_3)_n\cdot(CH_3CHO)_m\}H^+$ can be classified into two categories: (a) $n$ = 1 and $m$ = 2–4:

$$\{(NH_3)_n\cdot(CH_3CHO)_m\}H^+ \rightarrow \{(NH_3)_n\cdot(CH_3CHO)_{m-1}\}^+ + CH_3CHO \quad (8)$$

(b) $n$ = 2–11, $m$ = 1–4:

$$\{(NH_3)_n\cdot(CH_3CHO)_m\}H^+ \rightarrow \{(NH_3)_{n-1}\cdot(CH_3CHO)_m\}H^+ + NH_3 \quad (9)$$

The observed dissociation of cluster ion $\{(NH_3)_n\cdot(CH_3CHO)_m\}H^+$ is via only one channel, either reaction 8 or 9 but not both in our observable time window.

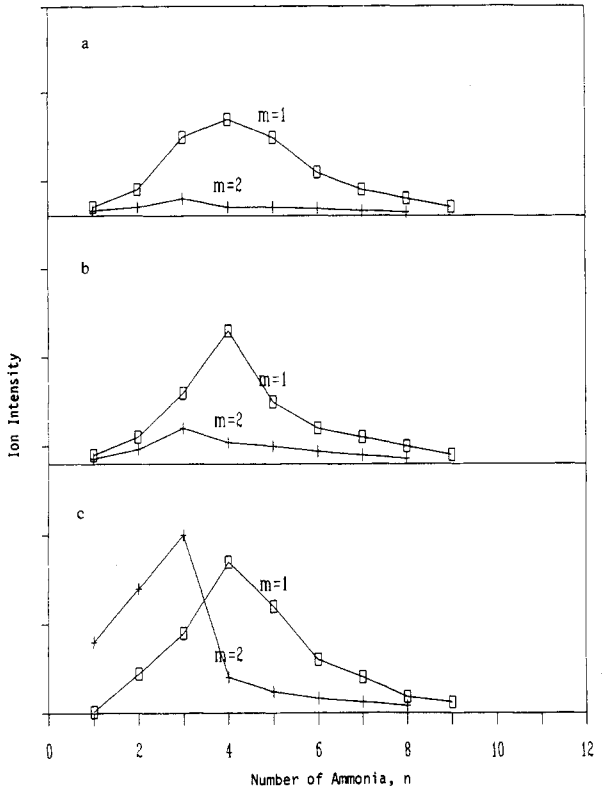


**Figure 10.** Plot of relative ion intensity of $\{(NH_3)_n\cdot(CH_3CHO)_m\}H^+$ as a function of $n$ for $m$ = 1–4. (a) $R$ = 1/4; (b) $R$ = 1; (c) $R$ = 4.

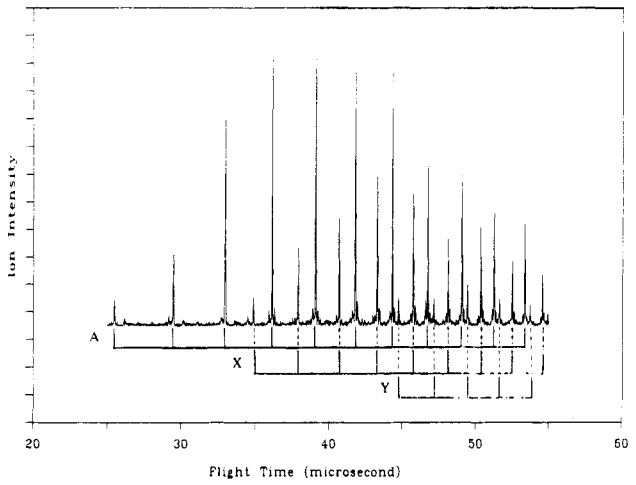


**Figure 11.** Daughter ion TOF spectrum of $\{(NH_3)_n\cdot(CH_3CHO)_m\}H^+$; $U_t$ = 1890 V. X, Y, Z, and W stand for daughter ion peaks with their corresponding parent ions $\{(NH_3)_n\cdot(CH_3CHO)_m\}H^+$, $m$ = 1–4, respectively. The metastable unimolecular decomposition processes expressed as (8) and (9) are discussed in the text.

## Discussion

Observing the loss pattern in a metastable unimolecular decomposition can serve as a qualitative way for probing a cluster ion structure.[43] Absence of metastable decomposition peaks in the reflectron TOF spectra indicates that the mixed protonated dimers $\{NH_3\cdot CH_3CN\}H^+$ and $\{NH_3\cdot CH_3CHO\}H^+$ are stable with respect to dissociation in the field-free region of our time-of-flight mass spectrometer. This is consistent with previous theoretical predictions.[44] The $\{NH_3\cdot CH_3CN\}H^+$ and $\{NH_3\cdot CH_3CHO\}H^+$ are expected to form linear hydrogen bonding bridges N···H···N and N···H·O. For many protonated dimers containing an ionic hydrogen bond, Moet-Ner[44] has proposed a correlation between the strength of the ionic hydrogen bond and the difference in the proton affinities of the two molecular species. It states that a smaller difference in the proton affinities of the two molecular species leads to a stronger hydrogen bond in the protonated dimer. As listed in Table II, the proton affinities of $NH_3$, $CH_3CN$, and $CH_3CHO$ ae 204.0, 189.2, and 186.6 kcal/mol, respectively.[45,46] Thus, hydrogen bonds in the $\{NH_3\cdot CH_3CN\}H^+$ and $\{NH_3\cdot CH_3CHO\}H^+$ are expected to be quite strong; the ions $\{NH_3\cdot CH_3CN\}H^+$ and $\{NH_3\cdot CH_3CHO\}H^+$ must be relatively stable. This is also in agreement with with thermochemical data where the enthalpies of the association reaction of $CH_3CN\cdot NH_4^+$ and $NH_3\cdot CH_3CNH^+$ are reported to be 27.6 and 43.2 kcal/mol, respectively.[47]

**TABLE II: Molecular Properties: PA ≡ Proton Affinity; $\mu$ ≡ Dipole Moment; $\alpha$ ≡ Polarizability**

| molecular species | PA,[a] kcal/mol | $\mu$,[b] D | $\alpha$,[c] Å$^3$ |
|---|---|---|---|
| $NH_3$ | 204.0 | 1.47 | 2.26 |
| $CH_3CN$ | 189.2 | 2.913 | 4.48 |
| $CH_3CHO$ | 186.6 | 2.70 | 4.59 |

[a] References 45 and 46. [b] Reference 48. [c] Reference 49.

The dissociation processes of $\{NH_3\cdot(L)_m\}H^+$, L = $CH_3CN$ or $CH_3CHO$, involve losing a L molecule as shown in processes (2) and (8). Since the proton affinity of $NH_3$ is higher than that of L, the proton is bound closer to the $NH_3$ than the L molecule within cluster ions. Hence, $\{(NH_3)_n\cdot(L)_m\}H^+$ can be written as $\{(NH_3)_{n-1}\cdot(L)_m\}NH_4^+$. It has been shown experimentally[11,16,28] and theoretically[29] that $(NH_3)_4\cdot NH_4^+$ is a particularly stable ion that can be pictured as a complete solvation shell formed by four $NH_3$ molecules bound to an ammonium core ion. The observation of the maximum in the ion intensity distribution of $\{(NH_3)_{n-1}\cdot(L)_m\}NH_4^+$ at $n + m = 5$ implies the existence of a stable and completed solvation shell. Therefore, the stable ions $\{(NH_3)_{n-1}\cdot(L)_m\}NH_4^+$, $n + m = 5$, can be pictured as a central ammonium ion $NH_4^+$ bound to four constituents in any combination of $NH_3$ and L molecules.

The decomposition channels of the metastable mixed parent cluster ions $\{(NH_3)_n\cdot(CH_3CN)_m\}H^+$ and $\{(NH_3)_n\cdot(CH_3CH)_m\}H^+$, $n$ = 2–11 and $m$ = 1–4, involve the loss of an ammonia molecule as expressed in processes (3) and (9). The experimental results can be explained by intermolecular interactions in a cluster. Therefore, consideration of the molecular dipole moment[48] and polarizability[49] can provide a qualitative prediction for intermolecular interactions within a cluster ion. Within a cluster ion, the ion–dipole interaction decreases as the square of the intermolecular distance while the ion–induced dipole decreases as the fourth power. Both dipole moment and polarizability for acetonitrile and acetaldehyde are greater than those for ammonia. See Table II. Considerations of the ion–dipole and ion–induced dipole interactions suggests that the metastable cluster ions $\{(NH_3)_n\cdot(CH_3CN)_m\}H^+$ and $\{(NH_3)_n\cdot(CH_3CHO)_m\}H^+$, $n$ = 2–11 and $m$ = 1–4, are expected to release the relatively loosely bound $NH_3$ molecule when undergoing evaporative unimolecular decomposition, just as is observed.

The observation of maximum intensities at $n + m = 5$ and the loss patterns of the unimolecular decompositions of cluster ions $\{(NH_3)_n\cdot(CH_3CN)_m\}H^+$ and $\{(NH_3)_n\cdot(CH_3CHO)_m\}H^+$ suggest that solvation shells are formed as depicted for structures I, where

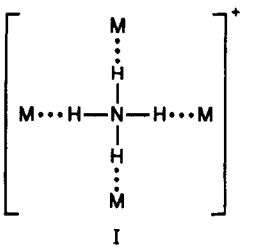


I

M is $NH_3$ or L (L = $CH_3CN$ or $CH_3CHO$) molecule. Similar experimental observations have been found in the mixed ammonia–acetone cluster system.[24,25]

## Conclusion

Local maxima in the relative ion intensity distributions of $\{(NH_3)_n\cdot(L)_m\}H^+$, L = $CH_3CN$ and $CH_3CHO$, at $n + m = 5$ are

found, indicating that the $\{(NH_3)_n\cdot(L)_m\}H^+$, $n + m = 5$, are particularly stable. It is proposed that a central ammonium ion $NH_4^+$ is bound to four constituents in any combination of ammonia and L molecules. Studies of metastable unimolecular dissociation processes reveal that the $\{(NH_3)_n\cdot(L)_m\}H^+$, $n = 1$, $m = 2-4$, cluster ions lose one L molecule whereas the $\{(NH_3)_n\cdot(L)_m\}H^+$, $n = 2-11$, $m = 1-4$, cluster ions lose one $NH_3$ molecule in a few tens of microseconds. The experimental results suggest that the stable cluster ions $\{(NH_3)_n\cdot(CH_3CN)_m\}H^+$ and $\{(NH_3)_n\cdot(CH_3CHO)_m\}H^+$, $n + m = 5$, have completed solvation shell structures as expressed in structures I.

*Acknowledgment.* Support by the U.S. Department of Energy, Grant No. DE-FG02-88-ER60668, is gratefully acknowledged.

**Registry No.** $NH_3$, 7664-41-7; $NH_4$, 14798-03-9; $CH_3CN$, 75-05-8; $CH_3CHO$, 75-07-0.

# Geometric and Electronic Structures of $C_{60}H_{60}$, $C_{60}F_{60}$, and $C_{60}H_{36}$

**B. I. Dunlap,* D. W. Brenner, J. W. Mintmire, R. C. Mowrey, and C. T. White**

*Theoretical Chemistry Section, Code 6119, Naval Research Laboratory, Washington, D.C. 20375-5000*
*(Received: February 8, 1991; In Final Form: March 13, 1991)*

Local density functional methods and empirical hydrocarbon potentials are used to study the electronic and geometric structures of icosahedral $C_{60}$, $C_{60}H_{60}$, and $C_{60}F_{60}$. Compared to isolated $C_{60}$, the C-H and C-F bond strengths of these saturated species are reduced by over 40% and over 15% from the C-H and C-F bond strengths in methane and in tetrafluoromethane, respectively. Similar C-H bond strengths are found for $C_{60}H_{36}$ and $C_{60}H_{60}$. Other $C_{60}H_n$ species are optimized by using empirical potentials. Outward bonding for all hydrogen atoms is not always energetically preferred.

## 1. Introduction

$C_{60}$ has been isolated in macroscopic quantities in several laboratories.[1-6] Carbon-13 NMR of pure $C_{60}$ dissolved in various solvents shows that this molecule has one symmetry inequivalent atom[3-5] and therefore has the proposed buckminsterfullerene (BF) structure with icosahedral ($I_h$) symmetry.[7] Haufler et al.[6] have partially hydrogenated $C_{60}$ using Birch reduction to yield $C_{60}H_{36}$. $C_{60}H_{36}$ is only the first in a series of new molecules that probably will be synthesized starting from $C_{60}$. Perhaps methods will be devised to fully hydrogenate $C_{60}$ to $C_{60}H_{60}$ and other routes found to yield $C_{60}F_{60}$, which should be inert similar to poly(tetrafluoroethylene). These hypothetical fully saturated $I_h$ molecules have already been studied theoretically within the Hartree-Fock (HF) approximation.[8] Stimulated by these results and possibilities, we have chosen to study the geometry and electronic structure of these and related molecules using empirical potentials[9] and local density functional (LDF) calculations.[10]

Of the many possible hydrogenated and fluorinated $C_{60}$ structures, the fully saturated species, $C_{60}H_{60}$, depicted in Figure 1, and the corresponding $C_{60}F_{60}$ molecule, have the highest symmetry and hence are easiest to study by the all-electron, first-principles LDF methods herein. However, if intermediate steps in the transformation of $C_{60}$ to $C_{60}H_{60}$ are considered, the high symmetry of the reactants and products is lost and a full geometry optimization of these intermediate species rapidly becomes impractical. In addition, if the proposed $C_{60}H_{36}$ structure,[6] depicted in Figure 2, is made from a molecular modeling kit using flexible tubes of roughly equal length to form nearest-neighbor bonds, then the bonds connecting saturated carbon atoms bend slightly inward while the bonds connecting unsaturated carbon atom pairs of their four neighboring saturated atoms are quite planar. The inward curvature of this model for these saturated C-C bonds is as great as the outward curvature of a similarly constructed $C_{60}$ molecule. The inward curvature for a fully saturated $I_h$ $C_{60}H_{60}$ is even greater. These results suggest that, rather than bonding all hydrogens to the exterior surface of the cage, lower energy isomers might be obtained by bonding a subset of these hydrogens to the interior surface of the molecule to better compensate local strains. However, putting one or a few hydrogen atoms inside the BF cage lowers both the tetrahedral ($T_h$) symmetry[11] of the proposed $C_{60}H_{36}$ structure[6] depicted in Figure 2 and the $I_h$ symmetry of the $C_{60}H_{60}$ molecule depicted in Figure 1, making a first-principles study of these isomers difficult. We have optimized the geometries of some of these lower symmetry structures using recently introduced empirical hydrocarbon potentials[9] as a practical way to address whether moving a subset of hydrogen atoms inside the $C_{60}$ cage lowers the total energy of these clusters. We also have used these empirical potentials in a preliminary survey of the energetics of hydrogen addition to the exterior surfaces of some of these clusters.

In section 2 we describe our LDF approach and compare our LDF results with experiment for $CH_4$ and $CF_4$. We also briefly review in section 2 our recently developed empirical hydrocarbon potentials. In section 3 we consider the icosahedral species, $C_{60}$, $C_{60}H_{60}$, and $C_{60}F_{60}$, with all H and F atoms bonded to the outside of the cage. Optimized LDF geometries allow us to compare the C-H and C-F bond energies of $C_{60}H_{60}$ and $C_{60}F_{60}$ and to compare empirical potential and LDF geometries for $C_{60}H_{60}$. In section 4 we use our LDF approach to study the recently synthesized,[6] partially hydrogenated species $C_{60}H_{36}$ at the optimized empirical potential geometry. In section 5 we consider a number of other $C_{60}H_n$ species using empirical potentials in a preliminary

* Corresponding author.

(1) Krätschmer, W.; Fostiropoulos, K.; Huffman, D. R. *Chem. Phys. Lett.* **1990**, *170*, 167.
(2) Krätschmer, W.; Lamb, L. D.; Fostiropolous, K.; Huffman, D. R. *Nature* **1990**, *347*, 354.
(3) Taylor, R.; Hare, J. P.; Abdul-Dada, A. K.; Kroto, H. W. *J. Chem. Soc., Chem. Commun.* **1990**, 1423.
(4) Johnson, R. D.; Meijer, G.; Bethune, D. S. *J. Am. Chem. Soc.* **1990**, *112*, 8983.
(5) Ajie, H.; Alvarez, M. M.; Anz, S. J.; Beck, R. D.; Diederich, F.; Fostiropoulos, K.; Huffman, D. R.; Krätschmer, W.; Rubin, Y.; Schriver, K. E.; Sensharma, D.; Whetten, R. L. *J. Phys. Chem.* **1990**, *94*, 8630.
(6) Haufler, R. E.; Conceicao, J.; Chibente, L. P. F.; Chai, Y.; Byrne, N. E.; Flanagan, S.; Haley, M. M.; O'Brien, S. C.; Pan, C.; Xiao, Z.; Billups, W. E.; Ciufolini, M. A.; Hauge, R. H.; Margrave, J. L.; Wilson, L. J.; Curl, R. F.; Smalley, R. E. *J. Phys. Chem.* **1990**, *94*, 8634.
(7) Kroto, H. W.; Heath, J. R.; O'Brien, S. C.; Curl, R. F.; Smalley, R. E. *Nature* **1985**, *318*, 163.
(8) Scuseria, G. E. *Chem. Phys. Lett.* **1991**, *176*, 423.
(9) Brenner, D. W. *Phys. Rev. B* **1990**, *42*, 9458.
(10) Dunlap, B. I.; Connolly, J. W. D.; Sabin, J. R. *J. Chem. Phys.* **1979**, *71*, 3396, 4993.
(11) Dunlap, B. I.; Brenner, D. W.; Mowrey, R. C.; Mintmire, J. W.; Robertson, D. H.; White, C. T. *Mater. Res. Soc. Symp. Proc.*, in press.